

# Change Detection in Urban Areas by Direct Comparison of Multi-view and Multi-temporal ALS Data\*

Marcus Hebel<sup>1</sup>, Michael Arens<sup>1</sup>, and Uwe Stilla<sup>2</sup>

<sup>1</sup> Fraunhofer Institute of Optronics, System Technologies and Image Exploitation IOSB,  
Gutleuthausstr. 1, 76275 Ettlingen, Germany

`{marcus.hebel,michael.arens}@iosb.fraunhofer.de`

<sup>2</sup> Department of Photogrammetry and Remote Sensing,  
Technische Universität München, 80290 München, Germany  
`stilla@tum.de`

\*This is the author's version of a paper published by Springer.  
The original publication is available at [www.springerlink.com](http://www.springerlink.com)

**Abstract.** Change detection in urban areas requires the comparison of multi-temporal remote sensing data. ALS (airborne laser scanning) is one of the established techniques to deliver these data. A novelty of our approach is the consideration of multiple views that are acquired with an oblique forward-looking laser scanner. In addition to advantages in terms of data coverage, this configuration is ideally suited to support helicopter pilots during their mission, e.g., with an obstacle warning system, terrain-referenced navigation, or online change detection. In this paper, we present a framework for direct comparison of current ALS data to given reference data of an urban area. Our approach extends the concept of occupancy grids known from robot mapping, and the proposed change detection method is based on the Dempster-Shafer theory. Results are shown for an urban test site at which multi-view ALS data were acquired at an interval of one year.

**Keywords:** airborne laser scanning, LiDAR, change detection, multi-temporal data analysis, urban areas

## 1 Introduction

### 1.1 Problem Description

Identification and analysis of changes in urban areas are common approaches to tasks like damage inspection, traffic monitoring, or documentation of urban development. Typically, changes of urban objects can be explained by human influences (e.g., construction, extension, or demolition of buildings). Moreover, seasonal effects (e.g., the foliage state of trees) and disasters (e.g., earthquakes) can cause considerable changes that occur on different time scales. Several types of changes are of interest when multi-temporal remote sensing data are compared. Typical categories include objects that have appeared, disappeared, moved (e.g., cars), transformed, or changed their spectral characteristics. Airborne laser scanning (ALS) is well suited to provide 3D measurements which allow direct comparison of geometric features. In this context, a basic requirement for detecting differences between multiple ALS point clouds is an accurate registration and alignment of the multi-temporal data.

Furthermore, additional requirements must be met by the data acquisition and data analysis if the laser scanner is used to support short-term operations such as the surveillance of urban areas, terrain-referenced navigation, or detection of rapid changes. Examples can be found in assistance systems for helicopter pilots, obstacle avoidance, landing operations in urban terrain, search and rescue missions, emergency services, or disaster management. These applications require methods for immediate processing of range measurements instead of the classical offline treatment of preprocessed ALS data.

## 1.2 Overview

Airborne laser scanning usually combines a LiDAR (light detection and ranging) device with highly accurate navigational sensors mounted on an aircraft. Typically, an IMU (inertial measurement unit) and a GNSS receiver (global navigation satellite system, e.g., GPS, the Global Positioning System) are operated synchronously with a LiDAR scanning mechanism.

The intention to use this sensor system for change detection implies that 3D data of the urban area in question had been acquired at an earlier date, so that currently measured ALS data can be compared to these. In this paper, we address change detection in the case that both the reference data and the current 3D data were acquired by an ALS system. In addition, we require this ALS system to allow access to the component's raw measurements, i.e., the range data, the scanning geometry, and the IMU/GNSS trajectory. In contrast to classical nadir data acquisition, we capture the scene with an oblique forward-looking laser scanner. This configuration is indispensable for some of the applications mentioned in Section 1.1. During acquisition of the reference data, multiple criss-crossing flight lines are used. Therefore, this setup has the additional advantage of full terrain coverage (e.g., facades of buildings etc.). Overall, we distinguish two different stages of ALS data acquisition and processing:

1. The creation of the database is not time-critical, i.e., the urban area can be scanned several times from multiple aspects with a calibrated sensor, while the data are processed and optimized offline. In (Hebel and Stilla 2007), we describe a method for the preclassification and the automatic registration of such ALS data.
2. During the mission, new ALS measurements are to be aligned and compared to the reference data. Regarding this task, we described a fast segmentation method in (Hebel and Stilla 2008) that is based on scanline analysis of ALS data. Matching of planar objects, which are identified in both the current data and the reference data, can be used to correct absolute errors of the sensor position (Hebel and Stilla 2010).

In this paper, we focus on the comparison step, and we start from the premise that the system calibration and data alignment issues are solved. Classical methods of change detection in ALS data typically compare the point clouds themselves. In contrast, we include knowledge on empty space that we observe during the data acquisition. With the assumption of a straight-lined propagation of laser pulses, we state that the space between the laser source and the reflecting 3D point must be empty (or transparent). Additionally, we allow for the occupancy of space behind the reflecting spot to be unknown, as long as it is not affected by other laser measurements. This consideration handles occlusions and changes implicitly, such that the latter are identifiable by conflicts of empty space and occupied space along the direction of the laser pulse (which we call henceforth "laser beam"). In robot mapping, such information is often managed in so-called occupancy grids. In this paper, we adapt some of these concepts for the use with 3D laser data. Instead of evaluating occupancy conflicts on raster cells, we identify these conflicts at the exact position of the 3D points. In the next section, we give an overview of related work on change detection and occupancy grids. Our own methodology is explained in Section 3. A description of our ALS setup and experimental results can be found in Section 4. Finally, Section 5 presents a brief discussion and our conclusions.

## 2 Related Work

In the last decades, change detection in urban areas has been explored by various groups. Most of them approach this task with different intentions and with different sensors. A typical example is the automatic update of building databases. In (Champion et al. 2009) some contexts and an evaluation of different approaches are described. In an overall analysis, it is concluded that LiDAR offers high economical effectiveness and represents a viable basis for future operative systems. The use of ALS for change detection with regard to buildings has been proposed, for instance, in (Murakami et al. 1999). Typically, a digital surface model (DSM) is generated by interpolating the 3D points onto a 2D

grid, and changes are detected by computing the difference of these DSM data. To increase reliability of the change detection results, Vögtle and Steinle (2004) classify the laser points into the classes bare-earth, building, and vegetation. We have described a similar classification approach in (Hebel and Stilla 2007) which is used to optimize the automatic registration of overlapping point clouds. The analysis of multi-temporal ALS data is sometimes proposed to assess damage to buildings, e.g., after earthquakes. Hommel (2009) puts strong emphasis on the elimination of vegetation in the ALS data, as this class of points could be misinterpreted, depending on the foliation state of the vegetation in the different data sets. A similar argumentation can be found in (Rutzinger et al. 2010), and it was confirmed in our experiments. However, other applications are conceivable wherein the detection and analysis of urban vegetation are of prime importance. A recent study on DSM-based change detection methods for urban areas and a detailed survey of related work can be found in (Matikainen et al. 2010).

Unlike the comparison of DSMs, the applications mentioned in Section 1.1 require a different strategy for data processing. There are two reasons for this: (i) we consider oblique views that lead to varying occlusions and point density depending on the aspect angle, (ii) the comparison of current ALS data to given reference data should be executable in line with the data acquisition.

Similar boundary conditions are given if ranging sensors are used on mobile robots (whose position and movement are known) in order to generate global maps from local and uncertain sensor data. Most commonly, 2D maps that are horizontal slices of 3D space, are taken as a basis. Moravec and Elfes (1985) were the first to represent these maps by an array of cells labeled *unknown*, *empty*, and *occupied*, with values ranging from 0 to 1 to define the “degree of certainty”. Puente et al. (1991) distinguish two different approaches to fuse information within such occupancy grids. These approaches are: (i) probabilistic estimation based on Bayes’ theorem, and (ii) the combination rule of the Dempster-Shafer theory of evidence (Shafer 1976).

Detailed work on autonomous navigation of mobile robots by a combination of probabilistic occupancy grids with neural networks was done by Thrun (1998). The evidence theory of Dempster-Shafer is commonly used for data fusion. In the context of occupancy models, it can substitute the probabilistic approach, and it has the additional advantage of evaluating conflicting information implicitly (Moras et al. 2011). In this paper, we evaluate such conflicts in multi-aspect and multi-temporal ALS data, which we organize in 3D raster cells. Similarly, Himmelsbach et al. (2008) proposed to use a  $2\frac{1}{2}$ D occupancy grid that acts like a hash table for the retrieval of 3D points. A description of the strengths and weaknesses of a 3D-based approach is given in the next paragraph.

### 3 Strategy for Data Processing

Two different operating modes of ALS data acquisition were explained in Section 1.2. In stage (1), a 3D voxel grid that covers the complete urban area is filled with information. During stage (2), we decide whether current ALS measurements confirm or contradict this information in the database. Fig. 1 illustrates such a 3D voxel grid and the process of ALS data acquisition. Within occupancy grids, the data are typically downsampled or interpolated to match the raster cells. Consequently, the details and positioning accuracy of detectable changes would be bounded by the resolution of the occupancy grid. On the other hand, a fine-grained 3D grid would lead to a huge amount of data.

Instead of evaluating the occupancy of space for the voxels themselves, we use the grid structure only to store information on the proximity of laser beams (and points). Once established, this data structure enables us to identify all candidates of old laser range measurements that may interfere with a new one. Furthermore, the cell size can be chosen comparatively wide (e.g., five times the average point-to-point distance), resulting in a moderate amount of data. Since the grid is only used as a search structure, the selection of the cell size has only minor impact on the results.

#### 3.1 Generation of the Database

In stage (1), each laser pulse’s origin  $\mathbf{s}$  is stored in an indexed list  $\mathbf{L}$ , together with the measured range  $\mathbf{r}$ , such that  $\mathbf{p} = \mathbf{s} + \mathbf{r}$  are the coordinates of the respective laser point. The sensor position

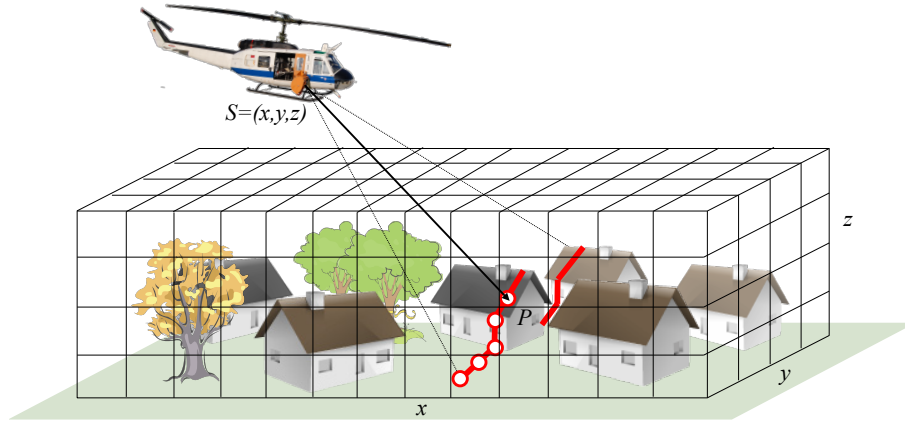


Fig. 1. ALS data acquisition and 3D voxel grid.

$\mathbf{s}$  and the direction of  $\mathbf{r}$  are interpolated from the synchronously recorded GNSS/IMU information which is typically captured with a frequency lower than the pulse repetition rate of the laser scanner. If multiple returns are received for a single laser pulse, these simply lead to multiple entries in  $\mathbf{L}$ . Furthermore, let  $\mathbf{r}_0$  denote the respective unit vector  $\mathbf{r}/\|\mathbf{r}\|$ . Two cell arrays  $\mathbf{V}_P$  and  $\mathbf{V}_R$ , both representing voxel grids as depicted in Fig. 2, are filled with indices of  $\mathbf{L}$  in the following way: Each index  $i \in \mathbf{L}$  is included in a single cell of  $\mathbf{V}_P$  according to the 3D position of the laser point  $\mathbf{p}_i$  that corresponds to this index. Therefore,  $\mathbf{V}_P$  simply represents a rasterization of the point cloud. Beyond that,  $\mathbf{V}_R$  is used to store all indices of laser beams that traverse the voxels. To cope with this task, we implemented a 3D variant of Bresenham's algorithm, that is well-known in computer graphics for efficient raster line drawing. For a single laser range measurement  $(\mathbf{s}_i, \mathbf{r}_i)$ , Fig. 2 illustrates how its index  $i$  is distributed among cells of  $\mathbf{V}_P$  and  $\mathbf{V}_R$ . Each cell in  $\mathbf{V}_P$  or  $\mathbf{V}_R$  can receive either none, one or multiple indices, depending on the number of laser points contained in this voxel, or depending on the number of laser beams that run through this voxel, respectively.

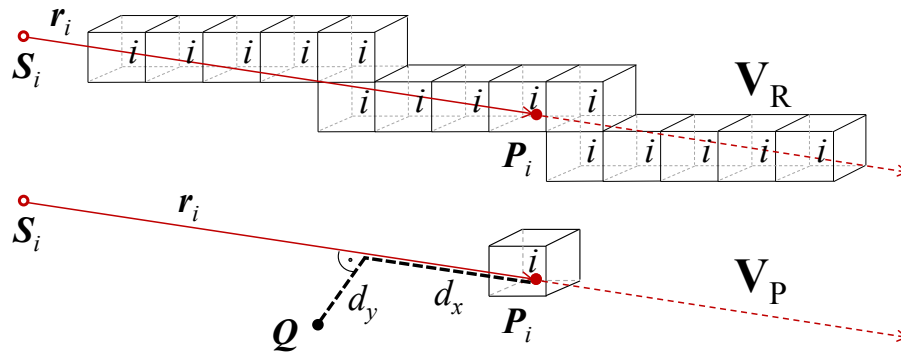


Fig. 2. Distribution of an index  $i$  among cells of  $\mathbf{V}_P$  and  $\mathbf{V}_R$ .

### 3.2 Modeling the Occupancy of Space

Following the terminology of the Dempster-Shafer theory, let  $U$  denote the universal set that contains all possible states of the observed system. In our case, we observe the occupancy of space at a given 3D position, so  $U = \{emp, occ\}$  is the universal set, where  $emp$  and  $occ$  are abbreviations for “empty”

and “occupied”. The power set  $2^U$  of  $U$  is given as the set  $\{\emptyset, \{emp\}, \{occ\}, U\}$ . A so-called belief mass in the interval  $[0, 1]$  is assigned to each element of this power set, with the additional properties that the empty set  $\emptyset$  has zero mass, and the sum of all other masses is one:

$$m : 2^U \rightarrow [0, 1], \quad m(\emptyset) = 0, \quad \sum_{A \in 2^U} m(A) = 1 . \quad (1)$$

An assignment that fulfills these criteria is called “basic belief assignment”. The Dempster-Shafer theory makes use of the mass assignments to define upper and lower bounds of an interval that contains the classical probability. These bounds are called “plausibility” and “belief”. Except for equation (1), the value of  $m(U)$  does not concern  $\{emp\}$  or  $\{occ\}$  itself, as each of these has its own mass. Instead, the mass  $m(U)$  of the universal set  $U$  is interpreted as the degree of ignorance. If  $m(U)$  equals one, this means that the occupancy of space at the given position is totally unknown. We model the impact of a laser range measurement  $\mathbf{p} = \mathbf{s} + \mathbf{r}$  on the assignment of masses to a position  $\mathbf{q}$  in 3D space in the following way: First, let  $d_x$  denote the longitudinal distance of  $\mathbf{q}$  to  $\mathbf{p}$  (cf. Fig. 2):

$$d_x = (\mathbf{q} - \mathbf{p}) \cdot \mathbf{r}_0 . \quad (2)$$

Similarly, let  $d_y$  denote the transverse distance of  $\mathbf{q}$  to  $\mathbf{p}$ :

$$d_y = \|(\mathbf{q} - \mathbf{p}) \times \mathbf{r}_0\| . \quad (3)$$

On the basis of the distances  $d_x$  and  $d_y$ , we define the following belief masses (at position  $\mathbf{q}$  caused by  $\mathbf{p}$ ):

$$\begin{aligned} m_{\mathbf{q},\mathbf{p}}(\emptyset) &= 0 , \\ m_{\mathbf{q},\mathbf{p}}(\{emp\}) &= \left(1 - \frac{1}{1 + e^{-\lambda d_x - c}}\right) \cdot e^{-\kappa d_y^2} , \\ m_{\mathbf{q},\mathbf{p}}(\{occ\}) &= \left(\frac{1}{1 + e^{-\lambda d_x - c}} - \frac{1}{1 + e^{-\lambda d_x + c}}\right) \cdot e^{-\kappa d_y^2} , \\ m_{\mathbf{q},\mathbf{p}}(U) &= 1 - m_{\mathbf{q},\mathbf{p}}(\{emp\}) - m_{\mathbf{q},\mathbf{p}}(\{occ\}) . \end{aligned} \quad (4)$$

By definition, (4) fulfills the conditions (1), so these equations represent a basic belief assignment. The respective first factor in  $m_{\mathbf{q},\mathbf{p}}(\{emp\})$  and  $m_{\mathbf{q},\mathbf{p}}(\{occ\})$  is composed of sigmoid functions. One of these is used to describe free space in front of  $\mathbf{p}$ , the other characterizes the lack of knowledge behind the laser point. In between, the inverse sum of the sigmoid functions reflects the actual occupancy at the position of  $\mathbf{p}$ . Fig. 3 shows the interaction of the sigmoid functions and the ratio of the belief masses along the laser beam, with the parameters in equations (4) set to  $\lambda=12$  and  $c=5$ . Outside of the beam axis, the second factor in  $m_{\mathbf{q},\mathbf{p}}(\{emp\})$  and  $m_{\mathbf{q},\mathbf{p}}(\{occ\})$  describes a Gaussian profile that fades to ignorance (transverse distribution). The parameters  $(\lambda, c, \kappa)$  describe the fuzziness of the laser points. They should be chosen to conform (at least) to the physical characteristics of the laser range measurements. This means that  $m_{\mathbf{q},\mathbf{p}}(\{occ\})$  should reflect the point positioning accuracy, which is influenced, for example, by the scanning precision and the range resolution of the specific laser scanning device. If  $m_{\mathbf{q},\mathbf{p}}(\{occ\})$  is too narrow, most range measurements would not interfere with another. Otherwise, if  $m_{\mathbf{q},\mathbf{p}}(\{occ\})$  is too broad, this would lead to false detections.

### 3.3 Combination of Evidence from Different Measurements

In the previous section we considered a single range measurement  $\mathbf{p} = \mathbf{s} + \mathbf{r}$  and its influence on the mass assignment to a position  $\mathbf{q}$ . In case we observe two or more laser beams in the neighborhood of  $\mathbf{q}$ , we need to combine the respective mass assignments. Let  $\mathbf{p}_1 = \mathbf{s}_1 + \mathbf{r}_1$  and  $\mathbf{p}_2 = \mathbf{s}_2 + \mathbf{r}_2$  be two independent laser range measurements. Equations (4) define different sets of mass assignments to the position of  $\mathbf{q}$ , which are given by  $m_{\mathbf{q},\mathbf{p}_1}$  and  $m_{\mathbf{q},\mathbf{p}_2}$ , respectively. For better readability, we abbreviate  $m_{\mathbf{q},\mathbf{p}_1}(\{emp\})$  to  $m_1(e)$  and  $m_{\mathbf{q},\mathbf{p}_1}(\{occ\})$  to  $m_1(o)$  etc.

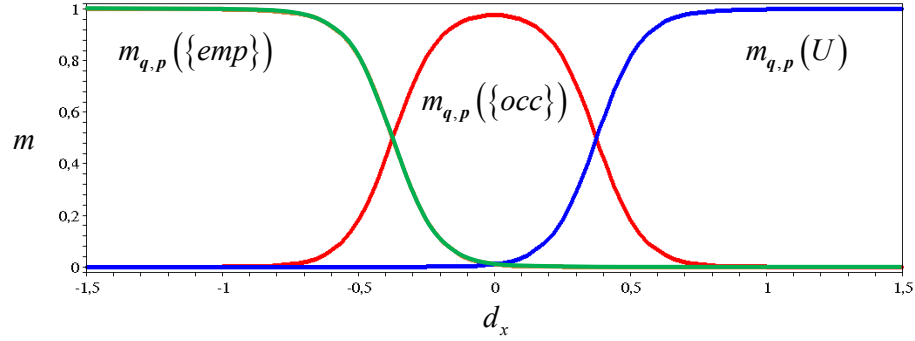


**Fig. 3.** Belief assignment to points on the laser beam ( $d_y = 0$ ).

Using these notations, we apply Dempster's rule of combination to calculate the joint mass  $m$  from the sets  $m_1$  and  $m_2$ . The amount of conflict  $C$  between the two mass sets is measured as follows ("empty in  $m_1$  and occupied in  $m_2$ , or vice versa"):

$$C = m_1(e) m_2(o) + m_1(o) m_2(e) . \tag{5}$$

Within Dempster's rule of combination, conflicting evidence is ignored, which is achieved by the normalization factor  $(1 - C)$  as follows:

$$\begin{aligned} m(e) &= \frac{m_1(e) m_2(e) + m_1(e) m_2(U) + m_1(U) m_2(e)}{1 - C} , \\ m(o) &= \frac{m_1(o) m_2(o) + m_1(o) m_2(U) + m_1(U) m_2(o)}{1 - C} , \\ m(U) &= \frac{m_1(U) \cdot m_2(U)}{1 - C} , \\ m(\emptyset) &= 0 \end{aligned} \tag{6}$$

The operations (6) are commonly written as  $m = m_1 \oplus m_2$  and result in a new set  $m$  of belief masses that is a combination of  $m_1$  and  $m_2$ . It should be noted that  $\oplus$  is commutative and associative. Therefore, even an arbitrary number of belief assignments can be combined by  $\oplus$  in a unique way.

### 3.4 Change Detection

In stage (2), we decide whether a new ALS measurement  $\mathbf{q} = \mathbf{s}_Q + \mathbf{r}_Q$  confirms or contradicts the mass assignments which we obtain from old measurements that we recorded in  $\mathbf{L}$ . Conflicts occur if the laser beam  $(\mathbf{s}_Q, \mathbf{r}_Q)$  traverses *occupied* space in front of  $\mathbf{q}$ , or if  $\mathbf{q}$  comes to lie in a region that is marked *empty*.

We address the latter case first. Let  $v_{\mathbf{q}} \subset \mathbf{V}_{\mathbf{R}}$  denote the cells of  $\mathbf{V}_{\mathbf{R}}$  which correspond to the position of  $\mathbf{q}$ . This subset  $v_{\mathbf{q}}$  may comprise only the voxel that includes  $\mathbf{q}$ , or an additional neighborhood. It is expected that  $v_{\mathbf{q}}$  contains the indices of laser beams in  $\mathbf{L}$  which may affect the mass assignment to the position of  $\mathbf{q}$ . Let  $I_{\mathbf{q}}$  be the set of indices which are associated with  $v_{\mathbf{q}}$ . On the one hand, we consider the joint mass  $m_{\mathbf{q}}$  resulting from all measurements  $\mathbf{p}_i$  in  $\mathbf{L}$  where  $i \in I_{\mathbf{q}}$ :

$$m_{\mathbf{q}} = \bigoplus_{i \in I_{\mathbf{q}}} m_{\mathbf{q}, \mathbf{p}_i} . \tag{7}$$

On the other hand, the mass assignment  $m_{\mathbf{q}}^*$  that we obtain from  $\mathbf{q} = \mathbf{s}_Q + \mathbf{r}_Q$  itself is given as:

$$m_{\mathbf{q}}^*(\{emp\}) = m_{\mathbf{q}}^*(U) = m_{\mathbf{q}}^*(\emptyset) = 0, \quad m_{\mathbf{q}}^*(\{occ\}) = 1 . \tag{8}$$

Based on these assignments, we can identify conflicts between  $m_{\mathbf{q}}$  and  $m_{\mathbf{q}}^*$  in the same way as it is done in equation (5), resulting in a measure of conflict  $C_{\mathbf{q}} = m_{\mathbf{q}}(\{emp\})$ .

The other type of conflict is caused by occupied space that is encountered while the laser pulse propagates from  $\mathbf{s}_{\mathbf{q}}$  to  $\mathbf{q}$ . To find these conflicts, we extend the list  $\mathbf{L}$  to include mass assignments to every point  $\mathbf{p}$  in  $\mathbf{L}$ . We initialize these masses to an *unknown* occupancy:

$$m_{\mathbf{p}}(\{emp\}) = m_{\mathbf{p}}(\{occ\}) = m_{\mathbf{p}}(\emptyset) = 0, \quad m_{\mathbf{p}}(U) = 1 . \quad (9)$$

We use Bresenham's line drawing algorithm in 3D to identify grid cells in  $\mathbf{V}_{\mathbf{p}}$  that are affected by the laser beam  $(\mathbf{s}_{\mathbf{q}}, \mathbf{r}_{\mathbf{q}})$ . Let  $v_{\mathbf{p}}$  denote this subset of  $\mathbf{V}_{\mathbf{p}}$ , and let  $I_{\mathbf{p}}$  be the set of indices associated with  $v_{\mathbf{p}}$ . For every position  $\mathbf{p}_i$  with  $i \in I_{\mathbf{p}}$ , we update the mass set  $m_{\mathbf{p}_i}$  to the joint mass of  $m_{\mathbf{p}_i}$  and  $m_{\mathbf{p}_i, \mathbf{q}}$ :

$$m_{\mathbf{p}_i} \leftarrow m_{\mathbf{p}_i} \oplus m_{\mathbf{p}_i, \mathbf{q}} \quad \forall i \in I_{\mathbf{p}} . \quad (10)$$

After the laser scanning process has left the reach of a point  $\mathbf{p}$  in the database, we evaluate the accumulated mass assignment  $m_{\mathbf{p}}$  and its conflict to  $m_{\mathbf{p}}^*$ , which is given analogous to equation (8). We obtain  $C_{\mathbf{p}} = m_{\mathbf{p}}(\{emp\})$  as a measure of conflict.

### 3.5 Including Additional Attributes

If the proposed methods are applied to typical ALS data, vegetation is likely to cause conflicting belief masses. This is to be expected, since vegetation typically leads to laser points that are blurred and delocalized due to a large echo width. Some laser pulses penetrate the vegetation and mark this space *empty*. Others are reflected by the foliage, indicating the same space is partially *occupied*. Furthermore, vegetation is subject to seasonal changes. If the detection of such changes is of minor importance, it is advisable to treat vegetation in a different way than ground level, buildings, or other man-made objects. Besides full waveform analysis, local principal component analysis (PCA) and region growing are common approaches to ALS point classification. Since the generation of the database in Section 3.1 is not time critical, we derive an additional weighting factor from local PCA that increases the amount of  $m(U)$  for all measurements which relate to vegetation.

## 4 Experiments

The data that we analyzed for this study were acquired during field campaigns in 2008 and 2009, using a RIEGL LMS-Q560 laser scanner (version 2006) in combination with an Applanix POS AV 410 inertial navigation system. All sensors were attached to a helicopter of type Bell UH-1D. Our current experimental setup lacks online data access, so the experiments described in this section were conducted in a post-processing mode based on the stream of recorded raw data. With our configuration and settings, each scan line of the laser scanner covered a field of view of  $60^\circ$  subdivided into 1000 angular steps. The inclination angle of the laser scanner was set to  $45^\circ$  while flying with the helicopter's nose pitched down (Fig. 1). Due to aviation security reasons, the minimum flight level had to be restricted to 1000 ft. These boundary conditions led to laser strips with a width of 500 m and an average point-to-point distance of 0.5 m. In April 2008, a test site was approached in a cross pattern, resulting in an accumulated point cloud which includes 5,400,000 points with an average point density of 16 pts/m<sup>2</sup>. Fig. 4a shows a rendered visualization of these reference data, where each point is gray-value coded according to the echo amplitude, which is derived from full waveform analysis. The cell size of  $\mathbf{V}_{\mathbf{R}}$  and  $\mathbf{V}_{\mathbf{P}}$  was chosen to be  $2 \times 2 \times 2$  m<sup>3</sup>, resulting in two cell arrays of the dimensions  $300 \times 300 \times 50$  (which corresponds to  $600 \times 600 \times 100$  m<sup>3</sup>) to cover the area in question. After the distribution of  $\mathbf{L}$ -indices among these cells, the memory requirements of  $\mathbf{V}_{\mathbf{P}}$  and  $\mathbf{V}_{\mathbf{R}}$  amount to 1.1 GB in total. The test site was scanned again in August 2009, using the same sensors and a similar setting.

Based on the recorded data stream of a single strip (south-to-north), we successively applied the methods described in Section 3. The parameters  $(\lambda, c, \kappa)$  in equations (4) were set to  $\lambda=12$ ,  $c=5$ ,

$\kappa=8$  as shown in Fig. 3. First results of this experiment are depicted in Fig. 4b. Conflicts  $C_p \geq 0.5$  are shown in red (objects that have disappeared), whereas conflicts  $C_q \geq 0.5$  are colored yellow (objects that have appeared). In this example, vegetation obviously causes a lot of conflicts  $C_q$ , which can be ascribed to seasonal influences (April vs. August). As described in Section 3.5, we may derive additional attributes in an independent manner (e.g., local PCA, region growing) and classify the reference data in  $\mathbf{L}$  to the classes ground, vegetation, and building. In case we want to focus on man-made changes, this classification allows us to decrease the influence of data points in the vegetation class. The result is shown in Fig. 4c and Fig. 4d. In addition to the previous color-coding, green points now indicate that these are (most likely) part of an unchanged building. The remaining conflicts are mainly caused by moved cars, demolition, and newly constructed buildings.

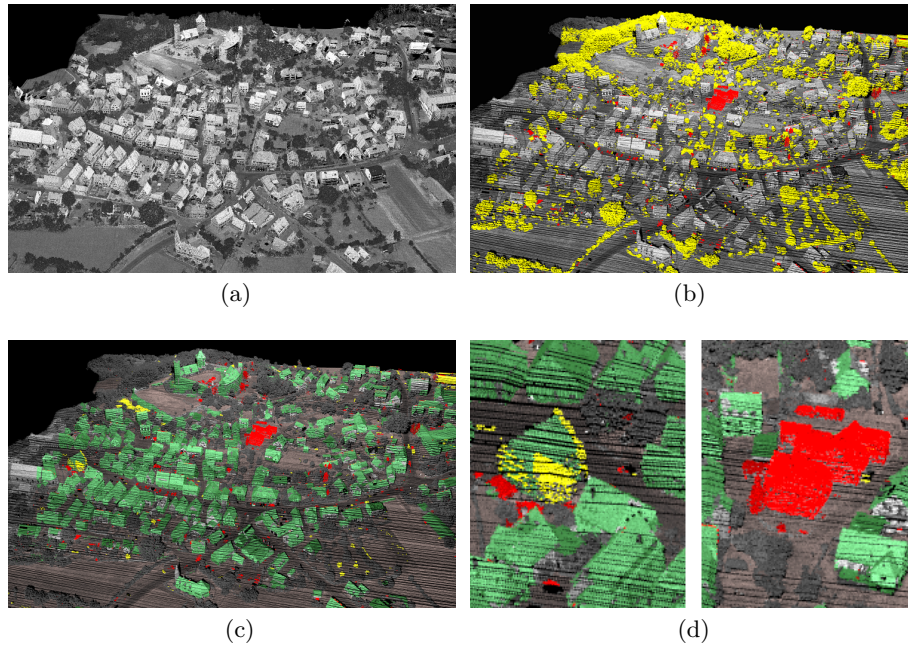


**Fig. 4.** (a) View of the reference data (April 2008), (b) conflicts of mass assignments (August 2009), (c) result of change detection, (d) close-up view

## 5 Discussion and Conclusion

In this paper, we have presented a framework for ALS-based change detection in urban areas. Our methodology is inspired by the concept of occupancy grids, and we implemented Dempster's rule of combination to fuse multiple measurements. During this process, conflicts between different belief assignments are evaluated with regard to change detection. The proposed methods are inherently realtime capable, as opposed to classical methods of point cloud analysis that start after the complete data set was obtained. Modern ALS instruments show a trend toward increasing performance and realtime processing. A typical example is online waveform analysis (e.g., RIEGL VQ-580). Furthermore, the presented techniques have high potential for parallelization, and the time-consuming evaluation of exponential functions can be replaced by look-up tables. We expect that an efficient implementation of the proposed methods can work in realtime on an operational system.

The main conceptual advantage of the proposed methods is the handling of occlusions as unknown space, which would otherwise require a more complex case-by-case analysis. In contrast to probabilistic approaches, the Dempster-Shafer theory allows an explicit representation of ignorance.

Therefore, even partially non-overlapping ALS data can be combined and compared without causing erroneously detections of changes. Different from the well-known concept of (2D) occupancy grids, we evaluate the occupancy of space at the discrete 3D positions of the laser points, without declining the given resolution of the laser scanner.

The experiments described in Section 4 demonstrated that spatial changes can be reliably detected, provided that the data are properly aligned. Seasonal changes in vegetation, changes of buildings (e.g., extensions, demolition), and moved cars are found by our automatic method. However, a few unresolved problems remain: For now, we ignored changes that occurred within the time slot in which the reference data were captured. The minimum size of detectable changes is limited by the point density and the respective point positioning accuracy, which need to be modeled correctly by means of the parameters  $(\lambda, c, \kappa)$ . A more quantitative evaluation is still missing, for which we would require the ground truth or simulated data. These issues will be part of our future work.

## References

- Champion, N., Rottensteiner, F., Matikainen, L., Liang, X., Hyypä, J., Olsen, B.P.: A Test of Automatic Building Change Detection Approaches. In: CMRT09, International Archives of Photogrammetry, Remote Sensing and Spatial Information Sciences 38 (3/W4), pp. 145–150. Paris (2009)
- Hebel, M., Stilla, U.: Automatic Registration of Laser Point Clouds of Urban Areas. In: PIA07, International Archives of Photogrammetry, Remote Sensing and Spatial Information Sciences 36 (3/W49A), pp. 13–18. München (2007)
- Hebel, M., Stilla, U.: Pre-classification of Points and Segmentation of Urban Objects by Scan Line Analysis of Airborne LiDAR Data. In: XXI ISPRS Congress 2008, Proceedings of Commission III. The International Archives of Photogrammetry, Remote Sensing and Spatial Information Sciences 37 (Part B3a), pp. 105–110. Beijing (2008)
- Hebel, M., Stilla, U.: LiDAR-supported Navigation of UAVs Over Urban Areas. In: Surveying and Land Information Science, Journal of the American Congress on Surveying and Mapping 70 (3), ISSN (printed) 1538-1242, ISSN (electronic) 1559-7202, pp. 139–149 (2010)
- Himmelsbach, M., Müller, A., Lüttel, T., Wünsche, H.-J.: LIDAR-based 3D Object Perception. In: Proceedings of 1<sup>st</sup> International Workshop on Cognition for Technical Systems. 7 p. München (2008)
- Hommel, M.: Verification of a Building Damage Analysis and Extension to Surroundings of Reference Buildings. In: Laserscanning'09, International Archives of the Photogrammetry, Remote Sensing and Spatial Information Sciences 38 (3/W8), pp. 18–23. Paris (2009)
- Matikainen, L., Hyypä, J., Ahokas, E., Markelin L., Kaartinen H.: Automatic Detection of Buildings and Changes in Buildings for Updating of Maps. In: Remote Sensing 2 (5), pp. 1217–1248 (2010)
- Moras, J., Cherfaoui, V., Bonnifait, P.: Moving Objects Detection by Conflict Analysis in Evidential Grids. In: Proceedings of the IEEE Intelligent Vehicles Symposium IV'11. Baden-Baden (2011)
- Moravec, H.P., Elfes, A.: High Resolution Maps from Wide Angle Sonar. In: Proceedings of the IEEE International Conference on Robotics and Automation, pp. 116–121. St. Louis (1985)
- Murakami, H., Nakagawa, K., Hasegawa, H., Shibata, T., Iwanami, E.: Change Detection of Buildings Using an Airborne Laser Scanner. In: ISPRS Journal of Photogrammetry and Remote Sensing 54 (2-3), pp. 148–152 (1999)
- Puente, E.A., Moreno, L., Salichs, M.A., Gachet, D.: Analysis of Data Fusion Methods in Certainty Grids - Application to Collision Danger Monitoring. In: Proceedings of the IEEE International Conference on Industrial Electronics, Control and Instrumentation, pp. 1133–1137. Kobe (1991)
- Rutzinger, M., Rüf, B., Höfle, B., Vetter, M.: Change Detection of Building Footprints from Airborne Laser Scanning Acquired in Short Time Intervals. In: ISPRS TC VII Symposium 100 Years ISPRS, International Archives of Photogrammetry, Remote Sensing and Spatial Information Sciences 38 (7b), pp. 475–480. Vienna (2010)
- Shafer, G.: A Mathematical Theory of Evidence. Princeton University Press. Princeton (1976)
- Thrun, S.: Learning Metric-Topological Maps for Indoor Mobile Robot Navigation. In: Artificial Intelligence 99 (1), pp. 21–71 (1998)
- Vögtle, T., Steinle, E.: Detection and Recognition of Changes in Building Geometry Derived from Multitemporal Laserscanning Data. In: XX ISPRS Congress 2004, International Archives of the Photogrammetry, Remote Sensing and Spatial Information Sciences 35 (B2), pp. 428–433. Istanbul (2004)